Visualizing motions within the cochlea's organ of Corti and illuminating cochlear mechanics with optical coherence tomography

Elizabeth S. Olson [a,*], Wei Dong [b], Brian E. Applegate [c], Karolina K. Charaziak [d],
James B. Dewey [d], Brian L. Frost [e], Sebastiaan W.F. Meenderink [f], Jong-Hoon Nam [g],
John S. Oghalai [d], Sunil Puria [h], Tianying Ren [i], C. Elliott Strimbu [j], Marcel van der Heijden [k]

[a] *Department of Otolaryngology - Head and Neck Surgery, Department of Biomedical Engineering, Columbia University, New York City, NY USA*
[b] *VA Loma Linda Healthcare System, Loma Linda, CA, USA, Department of Otolaryngology – Head and Neck Surgery, Loma Linda University Health, Loma Linda, CA USA*
[c] *Caruso Department of Otolaryngology -Head and Neck Surgery, Department of Ophthalmology, Department of Biomedical Engineering, University of Southern California, Los Angeles, CA USA*
[d] *Caruso Department of Otolaryngology - Head and Neck Surgery, University of Southern California, Los Angeles, CA USA*
[e] *The Rockefeller University, New York City, NY USA*
[f] *VA Loma Linda Healthcare System, Loma Linda, CA, USA*
[g] *Department of Mechanical Engineering, University of Rochester, Rochester, NY USA*
[h] *Massachusetts Eye and Ear, Harvard Medical School, Boston, MA USA*
[i] *Department of Otolaryngology - Head and Neck Surgery, Oregon Health and Science University, Portland, OR USA*
[j] *Department of Otolaryngology - Head and Neck Surgery, Columbia University, New York City, NY USA*
[k] *Department of Neuroscience, Erasmus Medical Center, Rotterdam, the Netherlands*

A B S T R A C T

Beginning in 2006, optical coherence tomography (OCT) has been adapted for use as a vibrometer for hearing research. The application of OCT in this field, particularly for studying cochlear mechanics, represents a revolutionary advance over previous technologies. OCT provides detailed evidence of the motions of components within the organ of Corti, extending beyond the first-encountered surface of observation. By imaging through the bony capsule as well as through the round window membrane, OCT has measured vibration at multiple locations along the cochlear spiral, in vivo, under nearly natural conditions. In this document, we present examples of recent research findings to illustrate the applications of OCT in studying cochlear mechanics in both normal and impaired ears.

1. Introduction

Optical coherence tomography (OCT) is a cross-sectional imaging technique that uses the natural contrast of back-reflected light to measure the intensity from microstructural features at various depths within biological tissues (Huang et al., 1991; Tearney et al., 1997). In 2006, two papers were published about developing the use of OCT for cochlear imaging and vibrometry (Choudhury et al., 2006; Hong and Freeman, 2006). The Choudhury et al. paper ended with the optimistic statement: " …there is a possibility that low-coherence interferometry can measure movements of the basilar membrane and reticular lamina in vivo with or without openings made into the bony wall of the cochlea." This ushered in what is now close to two decades of OCT-based measurements of intra-organ of Corti (OoC) motions, most made without opening the cochlea. Until the introduction of OCT, laser-based motion

measurements were made through either the round window (RW), or cochleostomies. Measurements were limited to the first surface that was encountered by the laser beam, the basilar membrane (BM) in the base, and Reissner's membrane, tectorial membrane (TM) or Hensen cells in the apex (Khanna and Hao, 1999; Robles and Ruggero, 2001). In this paper, we review a subset of recent measurements of intra-OoC motions made with OCT. The paper is mainly comprised of figures and accompanying text provided by researchers who are active in OCT-based intracochlear vibrometry. The last section of the paper is an extended list of papers from such studies.

In OCT imaging and vibrometry, four scan types are named, the "A-scan," "B-scan," "Volume-scan" and "M-scan." The fundamental scan is the A (axial)-scan. This is a one-dimensional (1-D) data set from points along the axis of the OCT light beam – the one dimension is depth into the preparation. The A-scan data are complex, having both magnitude

and phase. A B-scan is a 2-D "brightness" image, as in Fig. 1a. It is composed of a series of A-scans, taken as the scanning mirror shifts the beam perpendicular to the optical axis. The optical axis is along the vertical in the image plane with lower being deeper into the preparation. The magnitude of the A-scan data is presented as brightness values to form the B-scan. When a second mirror is scanned in the direction perpendicular to that of the first scanning mirror, a stack of B-scans is generated that can be viewed as a volume-scan. The axial resolution is determined by the light source bandwidth $\Delta\lambda$, and center wavelength λ_o, as $0.44\lambda_o^2/\Delta\lambda$. The lateral resolution of the B-scan image is determined by the numerical aperture of the objective lens.

To take vibration data, a single A-scan is recorded repeatedly at high rate (typically over 100 kHz). This is an "M-scan", for "motion scan." The A-scan pixels corresponding to structures of interest are then analyzed for the phase component of the A-scan data. The phase-versus-time of a given A-scan pixel is proportional to the structure's displacement – or more specifically, proportional to the component of the displacement that is projected onto the optical axis (vertical in the B-scan). For vibrometry, two types of OCT systems, spectral domain and swept source have been used. The two types differ in how they measure the reflectivity as a function of frequency. A spectral domain, or Fourier domain, OCT system (SD/FD OCT) uses a broad-band light source, typically a superluminescent diode, to simultaneously send all frequencies to the sample and reference mirror. The recombined light is passed through a spectrometer and the interference pattern is recorded with a line scan camera, typically a linear array of CCD detectors. A swept-source OCT system (SS OCT) uses a tunable laser source to quickly, typically a few hundred kHz per second, sweep through the frequencies. The recombined light can then be recorded with a single detector element and the interference pattern is measured by sweeping through all frequencies. Each of the two types has pros and cons. SS OCT systems can typically be operated at higher sampling rates and thus can scan faster than SD systems and typically produce higher image quality. SD systems have a finer axial resolution and higher signal-to-noise ratio at larger scanning depths. SS OCT systems' use of a tunable laser system introduces inherent phase jitter in the light and final "image". This can be challenging for vibrometry where the motion is encoded in the time-dependent phase of each pixel in the reconstructed scans. The OCT

instruments used for intra-OoC vibrometry fall into two camps – lab-built and commercially available systems from Thorlabs (Telesto and Ganymede). Both these camps are represented in the results reviewed here. A different but comparable system is the heterodyne low coherence interferometer developed by Ren (Fig. 3). Information on the development and use of OCT systems is in (Aumann et al., 2019; Applegate et al., 2011; Choudhury et al., 2006; Lin et al., 2019, 2017).

Intra-OoC measurements have provided a wealth of informative and provocative results related to how cochlear mechanics and amplification work, and creative theoretical work has followed (Altoe et al., 2022; Guinan, 2022; Samaras et al., 2023). However, in analyzing and conceptualizing the OCT results, new problems of interpretation have come to the forefront. In OCT instruments used for in vivo measurements, and thus with relatively long working distance objective lenses, OoC images are blurry, and the different anatomical structures only roughly distinguishable (Fig. 1a). Like laser Doppler vibrometry, OCT measures motion along the optical axis of the beam, vertical in a B-scan image. Pre-OCT, measurements of BM motion predominated, and BM motion is primarily in the transverse direction (Fig. 1b); then measurements taken from a non-transverse axis can be managed by a simple trigonometric multiplication. In contrast, intra-OoC structures, especially those in the region of the outer hair cells (OHC) apparently move in all three anatomical directions: radial, transverse, and longitudinal (Fig. 1b). To give an example of a resultant point of ambiguity: the reason for a structure's measured motion being small could be that its overall motion is small, but it could also be that the axis of vibration of the structure is nearly perpendicular to the optical axis. Also, due to the phase accumulation of the longitudinally traveling cochlear wave, the motion phase relationships between structures in a single A-scan will be influenced by their different longitudinal locations when the A-scan has a substantial longitudinal component. This issue, termed "skew", is the topic of one of the contributions below. This introduction serves to forewarn the reader that the interpretation of the OCT-based data is still in flux – it is a dynamic and stimulating time for the field of cochlear mechanics, and for unraveling the thread of cochlear amplification.

The first four contributions are observations of motion in the OoC and the fifth describes a method to account for skew. These are followed by two contributions that show changes in OoC motion due to
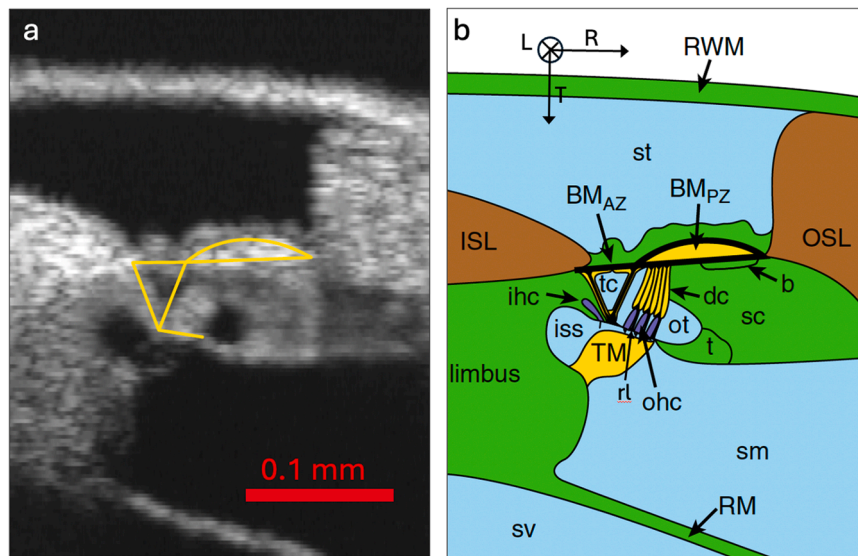
Fig. 1. (a) B-scan of basal region of gerbil cochlea through round window membrane. The optical axis is along the vertical, and the measured motions of structures are the overall motion of that structure, projected onto the optical axis. (b) Cartoon with the structures in the B-scan of (a) labelled. (b=Boettcher's cells, BM$_{AZ/PZ}$=basilar membrane arcuate and pectinate zones, dc=Deiters' cells, ISL=inner spiral lamina, ihc=inner hair cell, iss=inner spiral sulcus, ohc=outer hair cells, OSL=outer spiral lamina and ligament, ot=outer tunnel of Corti, RM=Reissner's membrane, RWM=round window membrane, sc=support cells, sm=scala media, st=scala tympani, sv=scala vestibuli, t=tectal cells, tc=tunnel of Corti (inner). L, R, T are the longitudinal, radial and transverse anatomical axes of the cochlea. Figure modified slightly from Cooper et al., 2018.

manipulations to the cochlea, one with furosemide administered to reduce endocochlear potential (EP), the other a mouse mutant in which a single row of OHCs has been deleted. Next, two contributions relate intra-OoC motion to otoacoustic emissions (OAEs). The final contribution is an in vitro study of the physical properties of OoC components, using a semi-intact gerbil cochlea.

2. Results

2.1. Complex motion patterns in the low-frequency region of the gerbil cochlea – Sebastiaan W.F. Meenderink & Wei Dong

OCT can penetrate the cochlear bony wall to assess cochlear function at various locations from intact cochleae. This includes the apical region of the cochlea—responsible for decoding low-frequency sounds that are crucial for human speech and sound perception. Fig. 2a shows a B-scan of the cochlear partition along the tonotopic (longitudinal) axis in the 2nd turn of the gerbil cochlea, where the best frequency (BF) varied between 2.1 and 2.8 kHz (Meenderink and Dong, 2022). The optical axis is vertical. By measuring the sound-evoked vibrations of the BM at multiple longitudinal locations, the traveling wave was tracked for individual frequency components in the stimulus. The wavelengths (Fig. 2b) were largest (~ 2.5 mm) for low-frequency tones and decreased to ~1 mm when the stimulus frequency was at, or slightly above, BF.

To complement this study in longitudinal variations, vibrations were recorded from different structures within the cochlear partition at a single longitudinal location. Fig. 2c shows a B-scan of such an "orthogonal" view (Meenderink et al., 2022), where different anatomical elements can be roughly discriminated (Fig. 2d). The optical axis is vertical in the B-scan and based on Fig. 2c had substantial radial and transverse components. Combining vibratory responses from multiple closely spaced recording locations within this image, a pair (amplitude and phase) of vibratory maps was obtained for a single frequency (Fig. 2e). These maps reveal relative motions between structures within the cochlear partition and presumably describe the cochlear micro-mechanics that are important for the sensitive cochlear response. The amplitude exhibited variation with frequency and sound pressure

level (SPL), as illustrated by the frequency response curves for the BM and the OHC region (Fig. 2f). As in the cochlear base (shown in later figures), OHC responses were larger for sub-BF frequencies and consequently show a less-tuned response relative to the BM. Different from the base is the frequency range over which BM responses grew compressively, which extended at least two octaves below BF. It is notable that auditory nerve tuning better resembled BM than OHC tuning (Fig. 2g).

As noted throughout this paper, knowing the OCT measurement angle relative to the (unknown) direction of a structure's motion is key for a proper interpretation of the data, and current research efforts are directed at obtaining 2-D or 3-D vibratory information in resolving this issue (for example, section 2.5 below). For 1-D measurements, the motion's projection onto the OCT beam has a pronounced effect on the measured amplitude and phase. Returning to the longitudinal study of Figure 2a&b, in Fig. 2h, the phase of OHC re: BM is shown as the beam (optical axis, vertical in the image) was moved from more basal to more apical locations (Fig. 2a). The phase shown in Fig. 2h had an almost bimodal dependence on the angle between the OCT measurement beam and the (longitudinal) curvature of the BM, switching from ∼ 0.25 to ∼ −0.25 cycle at the point where the beam axis was perpendicular to the longitudinal axis of the cochlea. The phase switch could result from predominantly longitudinal motion in the OHC region that was projected on the OCT optical axis (Meenderink and Dong, 2022) – the switch occurs as the projected motion switches from "towards the OCT system" to "away from the system". In addition, the measurement angle *re.* the longitudinal axes results in "skew", where structures at different positions along the A-scan are at different tonotopic locations. Section 2.5 below addresses this issue, and methods to account for it. In these apical data (Fig. 2), skew is of less consequence, as the OCT beam and the longitudinal BM axis are close to perpendicular, and the wavelengths are relatively long. The significance of OCT-based observations of OHC active mechanics to hearing requires a refined interpretation, especially in terms of motion direction and spatial resolution. Such refinement is needed to use these observations to discount or support hypotheses related to the mechano-sensation in the mammalian ear.
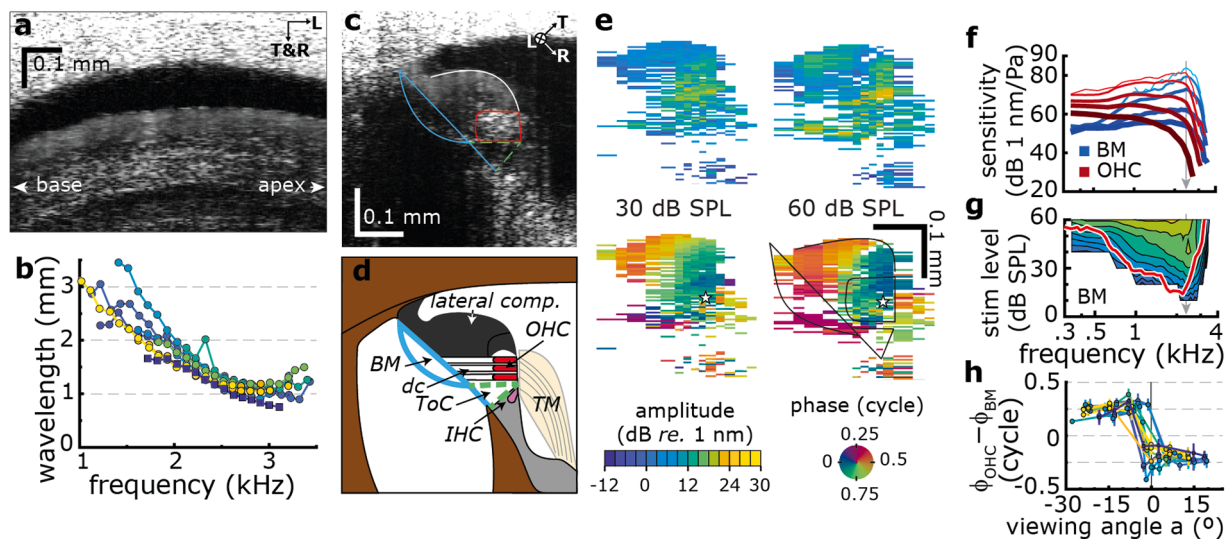
Fig. 2. Tone-induced responses at the 2nd turn of gerbil cochlea. (a) B-scan of cochlear partition along the tonotopic axis in the 2nd turn of the gerbil cochlea. The optical axis is vertical. L, R, T indicate anatomically based longitudinal, radial and transverse (perpendicular to BM) directions. (b) Wavelength of the traveling wave, calculated from phase measurements along the longitudinal, tonotopic axis of the cochlea. (c) B-scan of a cross-section of the cochlear partition. The optical axis is vertical. (d) Schematic of the anatomical structures in (c). (e) 2-D vibrometry maps (amplitude and phase) at the BF of 2.4 kHz for 30- and 60-dB SPL, respectively. Top and bottom plots are amplitude and phase respectively. (f) Sensitivities (amplitude normalized to stimulation) of the BM and OHC at different stimulus levels (20–60 dB SPL). (g) Iso-displacement map for the BM. For comparison, an auditory nerve fiber tuning curve (red) is superimposed (Schmiedt, 1989). (h) Variation of phase between the OHC and BM with changes in viewing angle re longitudinal axis. 0° is perpendicular to curved longitudinal axis in (a). Vibratory responses were obtained with a multitone stimulus (21 or 42 frequency components, 30–70 dB SPL); reported SPL are per component.

2.2. Relative motion between the reticular lamina and basilar membrane in the base of mouse and gerbil cochleae, measured with heterodyne low-coherence vibrometry – Tianying Ren

In common with OCT, heterodyne low-coherence interferometry (HLCI) also uses interference of low-coherence light to detect vibrations. While OCT measures vibrations by detecting sound-induced phase changes, HLCI detects the sound-induced Doppler frequency shift of the backscattered light. The HLCI technique has been used to measure reticular lamina (RL) and BM vibrations in mice and gerbils. The measurement locations within the cochlear partition are illustrated in Fig. 3a-c. Fig. 3d-k show RL and BM responses to tones in a mouse (Ren et al., 2016) and Fig. 3l shows RL and BM responses to clicks in a gerbil (He et al., 2018). While both BM and RL magnitude responses (Figs. 3d&g) showed sharp tuning and nonlinear growth, RL responses were larger than BM responses at all frequencies. The ratios of the BM and RL displacements to the malleus displacements (Figs. 3e&h) show that the RL nonlinear compression was stronger than that of the BM. The displacement ratios of RL to BM (Fig. 3j) illustrate how the RL vibrates more than the BM at all frequencies and SPLs. Near the BF of 48 kHz, low-level tone-induced RL vibration is about sevenfold larger than the BM vibration. This difference decreases with SPL and approaches one at 80 dB SPL. The largest magnitude ratio is at sub-BF frequencies.

The BM and RL phases (referred to the malleus vibration) decreased with frequency at an increasing rate (Fig. 3f&i). The phase difference at frequencies below 15 kHz was more than 90° and close to zero near 48 kHz (Fig. 3k solid black lines). The slope of the phase difference curves reveals a group delay of ~12 µs, which indicates that the RL vibrated after the BM vibration. The time relationship between the RL and BM vibration was also demonstrated by the click responses in Fig 3l. In response to a 10-µs rarefaction click, the RL moved toward the ST and reached the peak in ~0.41 ms, while the BM moved toward the SV and reached the maximum at ~0.38 ms. In contrast to BM *post mortem* responses, which only decreased in the BF peak, RL responses decreased across all frequencies (black dotted lines in Fig. 3d-h). Moreover, the ratio of the RL to BM displacement also decreased dramatically *post mortem* and approached one (dotted black lines in Fig. 3j), and the phase difference became almost zero (dotted black lines in Fig. 3k).

As in Fig. 2f of section 2.1, Figure 3 g&h show active sub-BF motion within the OoC that was not observed at the BM. Because of the sub-BF boosting of responses, these internal motions are less well tuned than BM. The tuning at the level of the auditory nerve is known to be like that of the BM, particularly at frequencies close to BF (Robles and Ruggero, 2001; Fig. 2g of section 2.1). The reduced tuning at locations within the OoC is puzzling, especially at the RL, which is close to the hair bundles. MET occurs due to pivoting motion at the stereocilia, and attempts have been made to determine that motion in vivo using OCT (e.g., Lee et al., 2016). Additional measurements, and cochlear modeling are needed to piece together the relationship between the currently measurable motions and the pivoting motion of the stereocilia.

2.3. Level-dependent motion patterns in the first turn of the gerbil cochlea – Marcel van der Heijden

Measurements were made through the RW membrane of the gerbil cochlea. This approach yields OCT images (B-scans) of the cochlear partition in the basal turn (Fig. 4a) in which the major anatomical structures can be identified (Fig. 4b). Because the orientation of the measurement beam (vertical in Fig. 4) was not aligned with any of the three anatomical axes (described in Fig. 1b), vibrometry recordings may contain contributions of motion along any of these directions. In the pre-OCT era, when most of the recordings were taken from the BM in the base of the cochlea, the actual direction of the motion had not been a concern; it was implicitly assumed that BM motion is transverse. With OCT it became possible to map the magnitude and phase across whole sections of the partition (Figs. 4c-h). The analysis of such vibration maps

strongly suggested that the motion inside the organ of Corti contains large contributions of motion along the longitudinal axis (Cooper et al., 2018). Such longitudinal motion was later confirmed and analyzed in more detail (Frost et al., 2023; Meenderink and Dong, 2022); see also sections 2.1 and 2.5.

There is another aspect of cochlear mechanics that became accessible with the advent of cross-sectional vibration maps. The maps show the spatial distribution of the vibration amplitude as heat maps. If one normalizes the amplitude to the maximum across the partition, as is done in Fig. 4, the map depicts the relative amplitude or "vibration mode" of the cross section. A fundamental question now arises: does the vibration mode change when the intensity of the sound is changed? In a linear system, vibrations are everywhere proportional to the stimulus, and the vibration mode would be invariant with sound intensity. It is well known that BM motion grows nonlinearly with sound intensity (Robles and Ruggero, 2001), and it is conceivable that the same amount of compressive nonlinearity would occur throughout the partition. Such a uniform nonlinearity would lead to one and the same vibration mode for all sound intensities. The early OCT measurements (e.g., Gao et al., 2014) already indicated that, in fact, nonlinear compression is not identical at different points within the cochlear partition. Normalized vibration maps provide a direct, quantitative assessment of the change of vibration mode with intensity. The maps in Fig. 4 show the normalized spatial response patterns for the best frequency (23 kHz) in the basal turn of the gerbil cochlea. The spatial distribution changes dramatically with increasing intensity: strongly focused near the OHCs (30–40 dB SPL); spreading towards the BM (50–60 dB SPL); migrating to the BM (70–80 dB SPL). The focus of motion in the OHC region, which is even more pronounced for frequencies well below the best frequency, introduced the term "hotspot" to the description of cochlear mechanics. Adapted from Figs. 2 and 3 of Cooper et al. (2018).

2.4. Reticular lamina vibrations in the very base of the gerbil cochlea – Nam Hyun Cho and Sunil Puria

Within the cochlea, the BM is coupled to the RL through three rows of piezoelectric-like OHCs and supporting cells, which work together to endow mammals with sensitive hearing. Using a Ganymede OCT system from Thorlabs, in vivo and *post mortem* displacements were measured through the gerbil RW from approximately the 40–47 kHz BF longitudinal location (Cho and Puria, 2022). The Ganymede has a shorter wavelength light source than the Thorlabs Telesto (900 nm versus 1300 nm center wavelength), and corresponding finer axial spatial resolution. The system allowed for measurements across the RL surface at individual OHCs within each of the three rows of OHCs. RL motion varied radially; at frequencies near the BF, the third-row gain was ~ three times greater than that of the first row (Figs. 5e & g), with a phase lead at sub-BF frequencies (Fig. 5h, compare red/green to blue curves). *Post-mortem*, the measured points moved together and approximately in phase (Fig. 5d & h). These results indicate that in vivo, the RL does not move as a stiff plate hinging around the pillar-cell heads near the first row, but that its mosaic-like structure bends and/ or stretches. Another notable aspect of these data is that the RL location lacked sub-BF boosting: post-mortem and in vivo responses lie together at frequencies less than ~ 0.7 BF (Fig. 5d). This is different from the pronounced sub-BF activity in intra-OoC motion seen in Sections 2.1 and 2.2. Cho and Puria (2022) did observe sub-BF activity at the OHC-Deiters cell location, and the explanation for the different results is likely that sub-BF activity is or can be quite localized within the OoC. The data shown in Fig. 5 are from a single animal and are representative data from the nine preparations included in the original paper.

2.5. Two issues arising from the uni-directional optical axis, and how to account for them – Brian L. Frost

In gerbil, measurements accessing the ~ 20 kHz BF location through
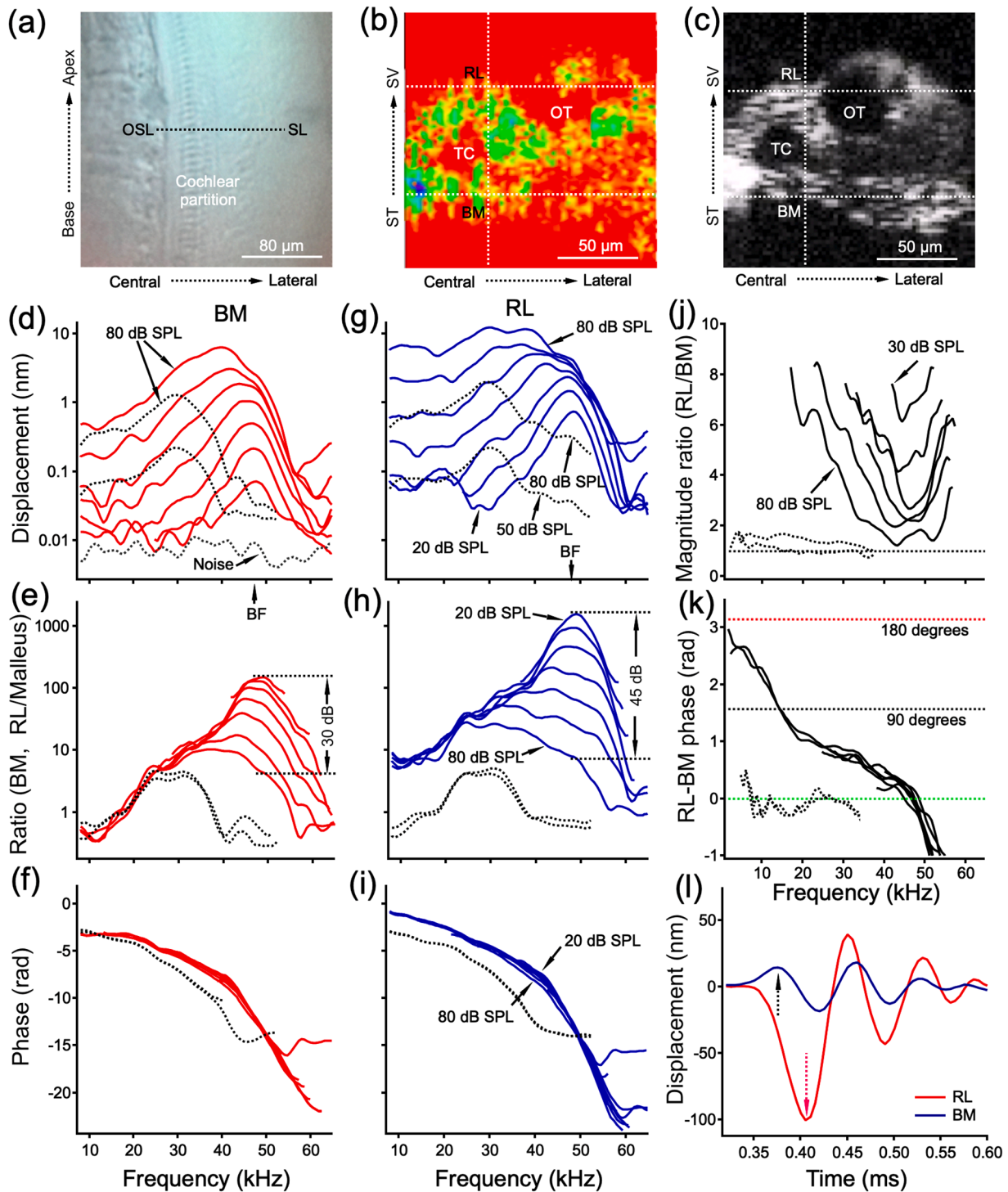
Fig. 3. The reticular lamina and basilar membrane vibrations in the basal turn of sensitive and insensitive cochleae. (a) Video still image of the cochlear partition through the RW in the basal turn of a living gerbil cochlea. OSL, osseous spiral lamina; SL, spiral ligament. Dotted line between OSL and SL indicates the scanning path for images in panels (b) and (c). (b) Image consisting of HLCI carrier signal level at each radial and transverse location. ST, scala tympani; SV, scala vestibuli; RL, reticular lamina; BM, basilar membrane; TC, tunnel of Corti; OT, outer tunnel. RL and BM vibrations were measured at the same radial location indicated by vertical dotted lines in panels (b) and (c). (c) An OCT B-scan image confirms the anatomical locations in panel (b). (d) BM displacement as a function of frequency at different SPLs. Data were collected under sensitive (solid red lines) and insensitive (dotted black lines) conditions. (e) Ratio of BM displacement to malleus displacement at different SPLs. (f) BM phase referred to the malleus vibration. (g) RL displacement as a function of frequency at different SPLs. (h) Ratio of RL displacement to malleus displacement. (i) RL phase referred to malleus vibration. (j) Magnitude ratio of RL vibration to BM vibration. (k) Phase difference between the RL and BM, obtained by subtracting the BM phase from the RL phase. (l) The RL (red) and BM (blue) responses to 10-μs rarefaction clicks at 90 dB SPL. The first peak of the BM displacement occurs >25 μs earlier than that of the RL vibration. Data in panels D-k were collected in a young CBA/CaJ mouse and those in panel l were collected in the basal turn of a sensitive gerbil cochlea. The mouse data were recorded through the intact RW membrane while the gerbil data were measured through a glass coverslip after the RW membrane was partially removed.
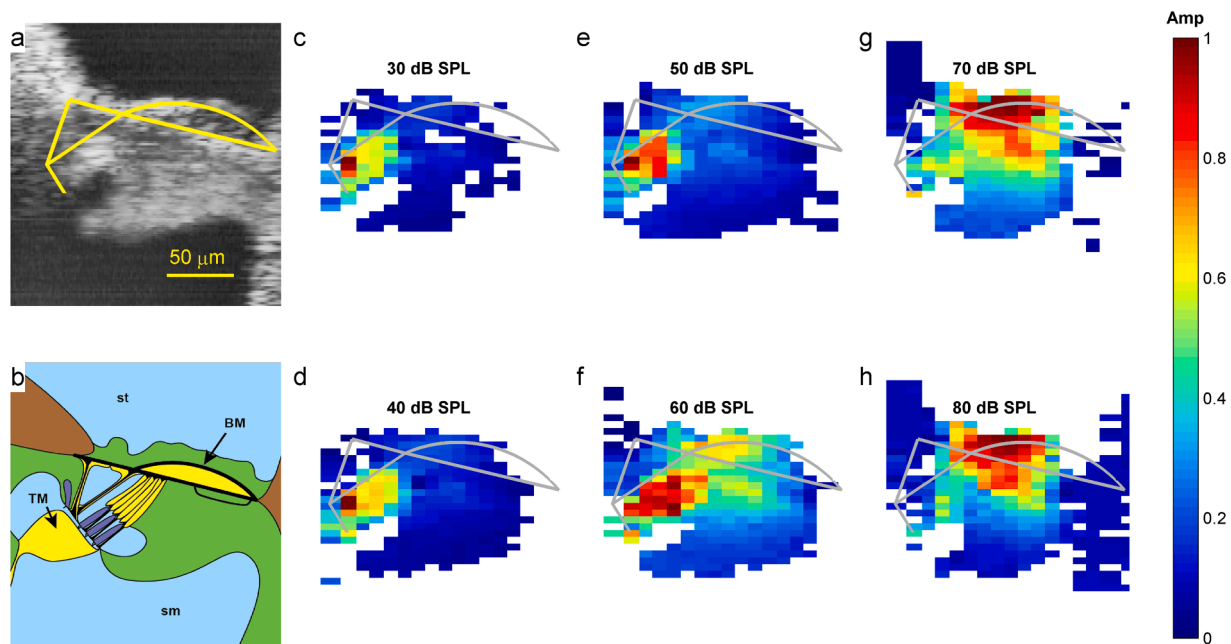
Fig. 4. The strong variation of vibration mode with sound intensity. The stimulus was a multitone (zwuis) complex with components ranging from 200 Hz to 38 kHz. Motion maps were constructed separately for each frequency component using Fourier analysis. Responses for each pixel were subjected to a Rayleigh test ($p =$ 0.001) for significant phase locking to the stimulus; only significant responses are shown. (a) OCT reflectance image (grayscale) with structural framework of Corti's organ (yellow) superimposed for reference. Basal turn (23-kHz region) of the gerbil cochlea; angle between the longitudinal axis of the basilar membrane and the optical axis, 53 deg. (b) Underlying anatomical structures. BM = basilar membrane; TM = tectorial membrane; st = scala tympani; sm = scala media. (c-h) Maps of vibration magnitudes, evoked by the 22.6-kHz component of a multitone stimulus (0.2–38 kHz). The intensity per tone was varied from 30 dB SPL (c) to 80 dB SPL (h) as indicated in the graphs. The colors represent the relative amplitude across each map, i.e. the linear vibration amplitude normalized to the maximum observed over all locations.

the RW require a significantly longitudinal optical axis, as illustrated in Fig. 6a. Along a single A-scan, the displacements at the BM (point 1) and OHC, Deiters cell junction (OHC-DC, point 2) were simultaneously measured. The two points are in different longitudinal cross-sections – a phenomenon termed skew. A second measurement was required to obtain BM (point 3) displacement measurements in the same longitudinal cross-section as OHC-DC point 2. This was done via a process termed skew correction, which uses a volume scan and analytic geometry to couple the anatomical axes to the system axes prescribed by the optical axis and scanning directions (Frost et al., 2022). Fig. 6b shows phase responses from the ~ 20 kHz BF location (expt. g900). BM and OHC-DC regions measured along the same optical axis (points 1 and 2, black and red curves of Fig. 6b) were approximately in phase at frequencies from ~ 16 to 25 kHz. After correcting for skew to compare BM and OHC-DC region phases within the same longitudinal cross-section (points 2 and 3, blue and red curves of Fig. 6b), OHC-DC phase was seen to lead BM across frequency.

When measuring from the more basal region adjacent to the RW (~ 45–50 kHz characteristic frequency (CF)), a transverse view is possible, so that a single A-scan traverses the BM and the OHC-DC region in the same longitudinal cross section, as in Fig. 6c. A phase response from this region is in Fig. 6d (expt. g961). The OHC-DC phase lagged BM across frequency. This at first seems at odds with the result in Fig. 6b, where the OHC-DC phase led BM, but the results can be understood in light of findings in the study of (Frost et al., 2023). There, the skew correction analysis was combined with a 2-D motion decomposition, in which motion at a single longitudinal location was measured with two different optical axes to find the longitudinal and transverse components of OHC-DC motion at that location. The components of OHC-DC motion were found to be similar in magnitude, but with different phase responses: the transverse motion lagged, and the longitudinal motion led the BM, across frequency. This explains the different phase responses in Figure 6b&d: The Figure 6b&d data were gathered with optical axes that

were primarily longitudinal or transverse, respectively. Thus, Fig. 6b captured the longitudinal component of OHC-DC motion (leading BM), and Fig. 6d captured the transverse component (lagging BM). This emphasizes the importance of reporting the optical axis angle alongside OCT micromechanical data.

2.6. Responses in the base of the cochlea with low and recovering endocochlear potential – C. Elliott Strimbu and Elizabeth S. Olson

Two experiments explored the recovery of cochlear activity following intravenous (IV) furosemide, a diuretic drug that reduces endocochlear potential (EP, the ~ +80 mV voltage within scala media that is partly responsible for driving current through the hair cells). In the initial set of measurements, recovery of activity was monitored with local cochlear microphonic (LCM), measured in scala tympani (ST) turn 1 (Fig. 7a) (Wang et al., 2019). LCM is a measure of local OHC transducer current. Fig. 7b shows the recovery of EP, which stabilized at a sub-normal value about 40 mins after the furosemide injection. The LCM BF peak was initially eliminated after furosemide, and recovery was poor at 39 min (when EP had already stabilized, Fig. 7c upper three panels). LCM recovery continued and was full at 100 min (Fig. 7c, lowest panel). Following furosemide the second harmonic of LCM increased. Fig 7d shows the response at the fundamental (stimulus) frequency (top panel) and the 2nd harmonic ÷ fundamental (bottom panel) as heat maps, with time on the vertical axis and stimulus frequency on the horizontal axis. (Here we show LCM normalized to the fundamental; the absolute level of LCM is also shown in Wang et al., 2019. Note: these responses were measured at 65 dB SPL, and the peak occurred at a slightly lower frequency than the ~ 17 kHz BF peak found at 30 dB SPL (Fig. 7c and d (top)).) The recovery of the LCM fundamental after about 80 min was accompanied by a reduction in LCM second harmonic. With a Boltzmann-type OHC MET curve representing the MET channels of OHC stereocilia, the increase of LCM second harmonic following
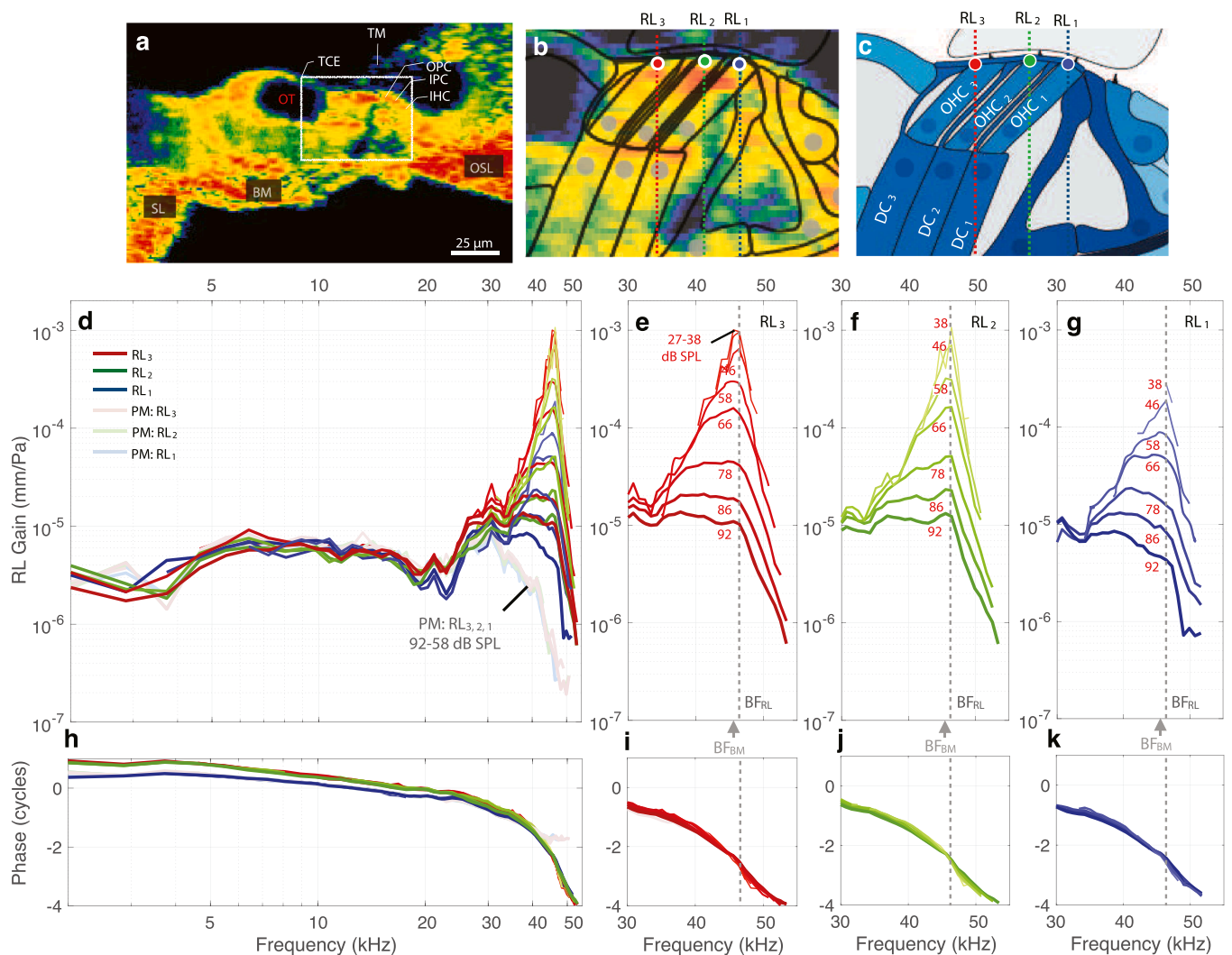
Fig. 5. The in vivo and *postmortem* RL gains across the apical ends of the three rows of OHCs (RL3, RL2, RL1) from gerbil G637. (a) A 2-D cross-sectional OCT image of a representative in vivo gerbil OoC with labeled key structures. The OoC structure is displayed "right side up" (with BM at the bottom) according to historical images. (b) An enlargement of the region in panel a within the white box, with overlaid line drawings of the cells and other structures, and details of the measurement locations across the apical ends of the three rows of OHCs (RL3, red circle; RL2, green circle; and RL1, blue circle). Each colored vertical line indicates the lateral position and direction of the different OCT A-scans for the OCT vibrometry measurements. (c) A labeled cross-sectional drawing from the 2-D OCT image in panel (b). (d) In vivo (dark red/green/blue) and PM (faded red/green/blue) gains for RL3, RL2, and RL1, respectively. (e–g) The in vivo, active-amplification region showing RL3, RL2, and RL1 gains, respectively. The gains were highest at low SPLs. The numbers in panels (e–g) indicate the stimulus level for each gain response (in panel e the curves overlap for 27–38 dB SPL). (h–k) The phase responses corresponding to panels (d–g). In this figure the displacements were normalized by the sound pressure to produce gains in units of mm/Pa, and the phase responses are in units of cycles. The frequency axis is on a log scale in panels (d) and (h), but on a linear scale in panels (e–g) and (i–k). (b) Overlaid line drawings and (c) cartoon drawing by Andrew A. Tubelli.

furosemide indicates that the MET operating point (OP) became less centered (Sirjani et al., 2004). The subsequent reduction in LCM 2nd harmonic indicates OP recentering, and the timing ties OP recentering to LCM recovery.

The LCM, furosemide experiment was followed up with an experiment where OoC motion was monitored with a Thorlabs Telesto OCT system (Fig. 7e-g, Strimbu et al., 2020). Displacement is shown at the BM and the OHC region (Fig. 7f). Initially both positions show a BF peak at $\sim$ 25 kHz, with nonlinearity at peak frequencies at the BM and wideband in the OHC region (Fig. 7e, top). Following IV furosemide the OHC-region motion was reduced and became low-pass and the BM peak was reduced and nearly linearized. Recovery of sub-BF responses in the OHC region was complete by 70 min, whereas BF peak responses recovered later, at about 120 min (Fig. 7e), a similar timescale as LCM recovery (Fig. 7c). $2f_1$-f_2 distortion product otoacoustic emission (DPOAE) responses are odd-order-distortions, predicted to be small or

large when MET OP is respectively off-centered or centered. They were reduced following furosemide and the DPOAE with $f_2 \sim$ 25 kHz recovered over $\sim$ 100 min, the same timescale as BF-peak recovery. Together, these findings suggest that recovery of MET, and thus recovery of some aspect of stereocilia mechanics, leads to the eventual recovery of cochlear amplification.

2.7. Responses in a genetically modified mouse cochlea – John S. Oghalai and Brian E. Applegate

Along the length of the cochlear duct, three rows of OHCs transduce the vibratory traveling wave and generate forces to amplify it. At the $\sim$ 10 kHz region in mice, while vibrations of the RL are amplified over a wide frequency range (Dewey et al., 2021; He et al., 2018; Lee et al., 2016; Ren et al., 2016), vibrations of the BM are only amplified by OHCs located within $\sim$1 mm of the peak of the traveling wave (Dewey et al.,
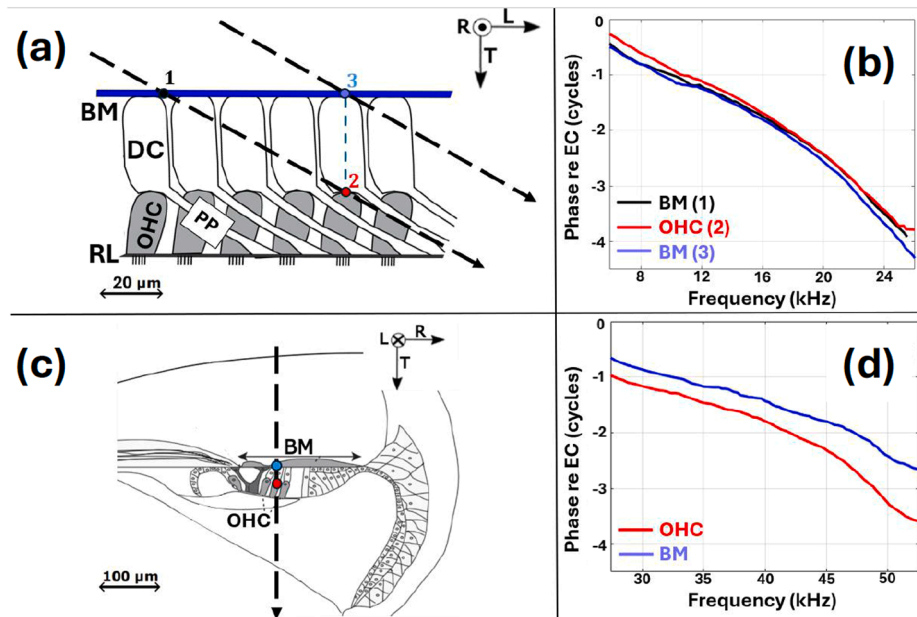
Fig. 6. Illustration of two ambiguities incurred by the viewing angle in OCT displacement measurements. (a) Cartoon of a longitudinal-transverse cross-section of the OoC complex when the optical axis has a substantial longitudinal component. Dashed black arrows show two OCT optical axes, each making a 60° angle with the BM normal, and circles indicate positions of interest. (b) Corresponding phase responses from a gerbil (g900) at the 22 kHz BF location. (c) Cartoon of a radial-transverse cross-section of the OCC, with a single OCT optical axis capturing a point on the BM and a point at the OHC-DC in the same longitudinal cross section. This beam axis is near-purely transverse. (d) Corresponding phase responses (g961 50 kHz BF).

2019). The mechanisms that underlie OHC force summation to create the high gain and sharp frequency tuning associated with cochlear amplification are important to understand because most forms of hearing loss experienced by patients are related to OHC loss.

Using OCT to image non-invasively through the otic capsule bone, we measured BM vibrations in $Lgr5^{DTR-EGFP/+}$ mice (Xia et al., 2022). The mice develop normally and have normal hearing. However, when injected with diphtheria toxin (DT) in adulthood their third row of OHCs and Deiters cells die off, creating a mouse with only two rows of OHCs. We studied non-injected control mice that have three OHC rows (Fig. 8 *left*) and DT-injected experimental mice that only have two rows of OHCs (Fig. 8 *right*).

The cochlear gain between 30 and 80 dB SPL at the frequency of maximal vibration was determined. In control mice, the gain was 18.8 ± 2.8 dB whereas it was markedly reduced to 5.3 ± 1.0 dB in experimental mice ($p = 0.002$). Also, frequency tuning was significantly broader in experimental than in control mice. We calculated the $Q_{10\,dB}$ to 30 dB SPL stimuli to assess the sharpness of BM vibration and frequency tuning. In control mice, the $Q_{10\,dB}$ was 2.02 ± 0.34 whereas it was 1.17 ± 0.12 in experimental mice ($p = 0.049$).

Thus, BM vibration in vivo demonstrated a reduction in cochlear amplification by about 13.5 dB This was disproportionate in that reducing OHC numbers by 33 % caused a gain to drop by 79 %. Because OHC forces progressively and sequentially amplify the traveling wave as it travels to its peak, the loss of even a relatively small number of OHCs over a spatial distribution will cause a substantial reduction in cochlear amplification. This means that OHC forces have compounding effects. Furthermore, this study demonstrates the power of combining OCT with transgenic mouse mutants to investigate complex pathophysiology in a targeted and non-invasive way.

2.8. Byproduct of cochlear nonlinearity, intracochlear distortion products and DPOAEs – James B. Dewey

OCT is a promising tool for examining how intracochlear motions lead to the generation of distortion-product (DP) OAEs – sounds transmitted to the ear canal as a byproduct of nonlinear cochlear amplification. Compared to previous measurements of the motion or pressure at the BM, OCT allows us to more directly relate DPOAEs to the motions of the OHCs, which are thought to generate the DPs. This may clarify the window that DPOAEs provide onto cochlear mechanics and OHC function, thus improving their diagnostic utility.

We recently studied how DPs are shaped as they are transmitted and propagated within the mouse cochlear apex (Dewey and Shera, 2023). At the ~9 kHz location (Fig. 9a-b), stimulation with two tones (at frequencies f_1 and f_2, $f_2 > f_1$) elicited intracochlear DPs that were measurable over a wide range of frequencies (Fig. 9c). Intracochlear DPs were typically strongest near the OHCs, though their absolute and relative magnitudes varied considerably across the OoC. Interestingly, only a few of these DPs were detectable in the ear canal as DPOAEs. While the dominant DP in the ear canal was usually $2f_1$-f_2, this was often not the largest DP observed in intracochlear vibrations.

The complex relationships among intracochlear and ear canal DPs are highlighted by fixing the f_2 frequency and varying f_1 (Fig. 9d). While intracochlear $2f_1$-f_2 DP magnitudes generally increased with decreasing f_2/f_1 ratio, they grew non-monotonically on the BM and TM, with magnitude valleys observed near f_2/f_1 ratios of ~1.3. In contrast, $2f_1$-f_2 DPOAE magnitudes exhibited a tuned, bandpass shape, peaking near an f_2/f_1 ratio of 1.3 and rapidly declining at larger and smaller ratios. The data therefore demonstrate that various factors strongly shape DPs as they are transmitted and propagated within the cochlea. These factors likely include variations of the mechanical properties of the cochlear structures and wave interference between DPs generated at different locations. Modeling results indicate that wave interference, in particular, is responsible for the bandpass shape observed in DPOAEs.

2.9. Organ of Corti vibrations and stimulus-frequency otoacoustic emissions – Karolina K. Charaziak

OAEs are sounds emitted by the inner ear spontaneously or in response to sounds. The presence of robust sound-evoked OAEs is a sign of functioning OHCs, which are responsible for the amplifying action of the OoC. For the past 50 years, the field has assumed that the motion of the entire OoC must follow the motion of the underlying BM, with
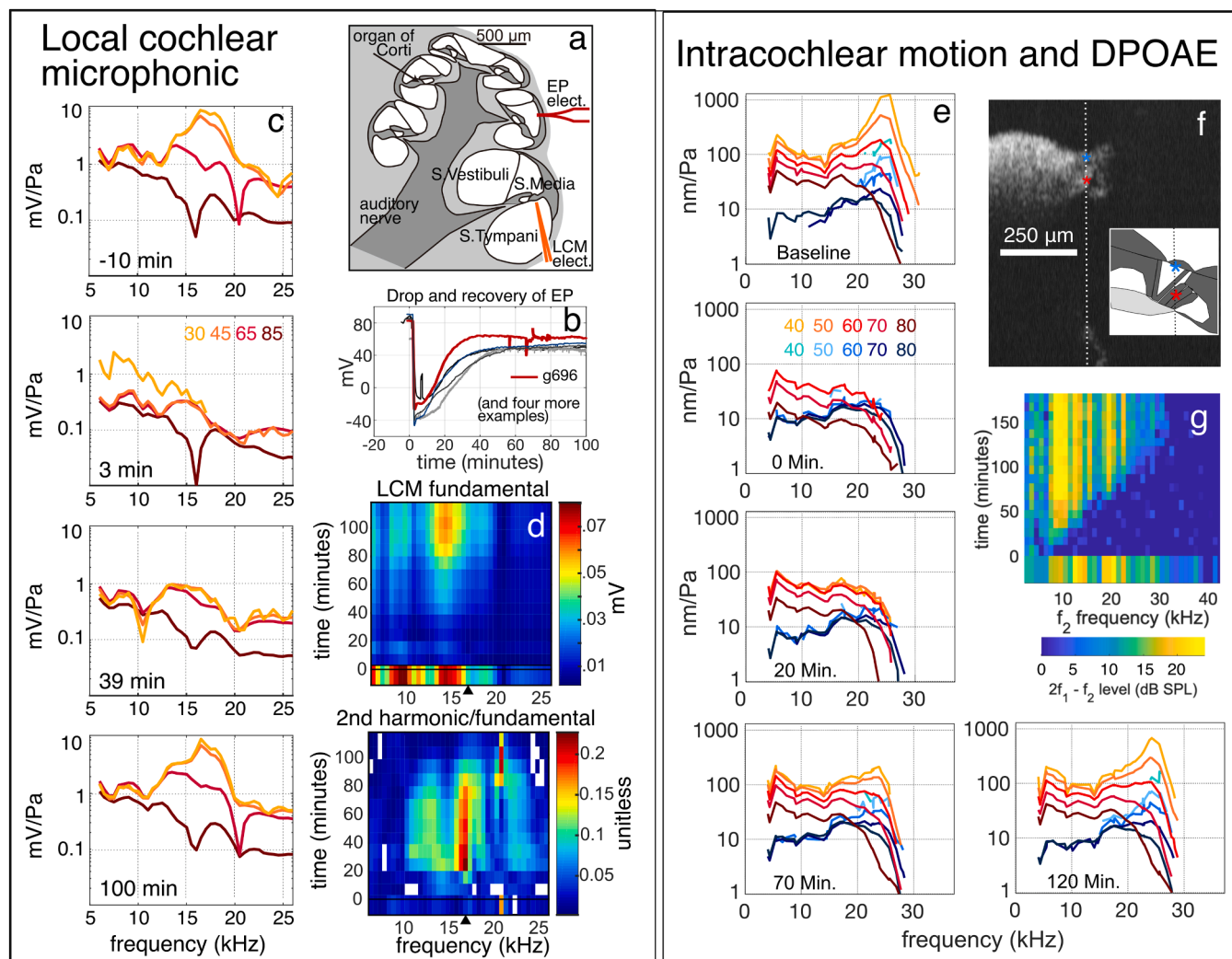
Fig. 7. Loss and recovery of turn-1 cochlear responses following intravenous (IV) furosemide in gerbil. (a-d) Experiment 1 (a) Set-up to measure endocochlear potential (EP) and LCM in the gerbil. (b) EP versus time following furosemide. Several preparations shown, red curve corresponds to the experiment of (c, d). (c) Four vertical panels show fundamental component of local cochlear microphonic (LCM) at different time points just prior to and following furosemide administration. The stimulus was pure tones at SPLs indicated in the second panel. (d) Two panels show LCM fundamental (top) and 2nd harmonic ÷ fundamental (bottom), measured at 65 dB SPL and plotted versus stimulus frequency. (The sharp increase at 20 kHz, 90 mins (bottom panel) is due to a notch in the fundamental (top and Fig. 7c) and is not of interest here.) (e-g) Experiment 2. (e) Five panels show intracochlear displacements at time points just prior to and following furosemide administration. Displacements of the OHC region are in reds; from the BM are in blues. (f) B-scan of probed location, with corresponding anatomical sketch. Vertical line in each indicates A-scan line and colored asterisks the locations of vibration measurements. (g) 2f₁-f₂ DPOAE responses versus time (50 dB primaries, f₂/f₁ ratio = 1.2).

mechanical properties that shape the frequency response of the inner ear. However, through revolutionary OCT recordings, we learned that not only do OoC vibrations differ from those of the BM, but the OHCs appear active in both the peak and the tail regions of the traveling wave (Cooper et al., 2018; Gao et al., 2014; Lee et al., 2016; Ren et al., 2016). This discovery requires us to revisit our BM-centric understanding of OAE generation.

Stimulus-frequency (SF) OAEs, evoked with pure tones, have long been considered as most promising in noninvasive evaluation of cochlear amplification near the peak of the traveling wave, although this view has been challenged (e.g., Siegel et al., 2005). Recordings of SFOAEs, however, are not straightforward and typically require an additional suppressor tone to extract the OAE suppression residual signal in the ear canal. The suppression residual represents the difference in the ear's response to a probe tone at frequency f_p due to presence of suppressor tone at a frequency f_s. This technique relies on two-tone suppression, where a cochlear vibration to the probe tone is reduced by the suppressor (e.g., Ruggero et al., 1992). To better understand how intracochlear suppression relates to SFOAE tests, we measured OoC and

BM vibrations in mice (CBA/CaJ) near the 9-kHz tonotopic location across a range of probe intensities (Charaziak, 2022; Charaziak and Pliso, 2023). When the suppressor tone was close in frequency to the probe ($f_s/f_p = 1.1$) BM and OoC vibrations at the CF were strongly reduced (Fig. 10a, b; red dashed) compared to vibrations measured with the probe tone alone (black solid). As a result, the BM and OoC suppression residuals at CF displayed characteristic compressive nonlinearity, with gain decreasing as probe intensity increased (Fig. 10c; dark to light). Similar behavior was observed for SFOAE residuals measure with a narrow ratio (Fig. 10e). These data support the view that SFOAEs measured with a narrow ratio reflect cochlear nonlinearity in the peak region of the traveling wave. However, with a wider ratio ($f_s/f_p = 2.1$), the BM response to the probe tone was minimally affected by the suppressor (Fig. 10a, black vs. dashed blue), yet strong SFOAEs were measured in the ear canal (Fig. 10f). When the suppressor frequency equaled CF, there was strong suppression of OoC vibrations (Fig. 10b, blue arrow), revealing a strong residual response (d, solid lines) that showed linear dependence on stimulus level, with gain independent of probe intensity. Similar behavior was observed for SFOAE residuals
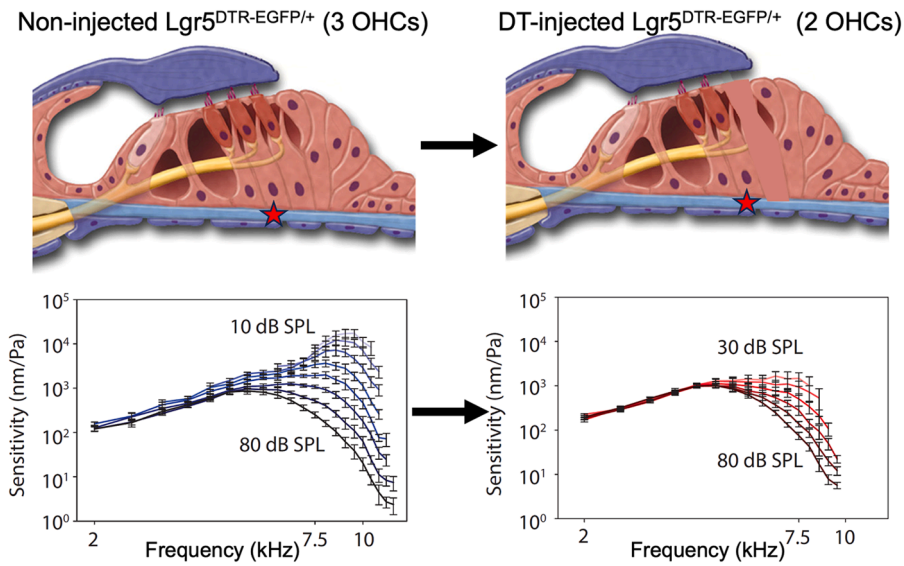
Fig. 8. Reduced cochlear amplification in a mouse mutant following elimination of one row of OHCs. The figure was taken from a published graphical abstract (Xia et al., 2022) and modified.
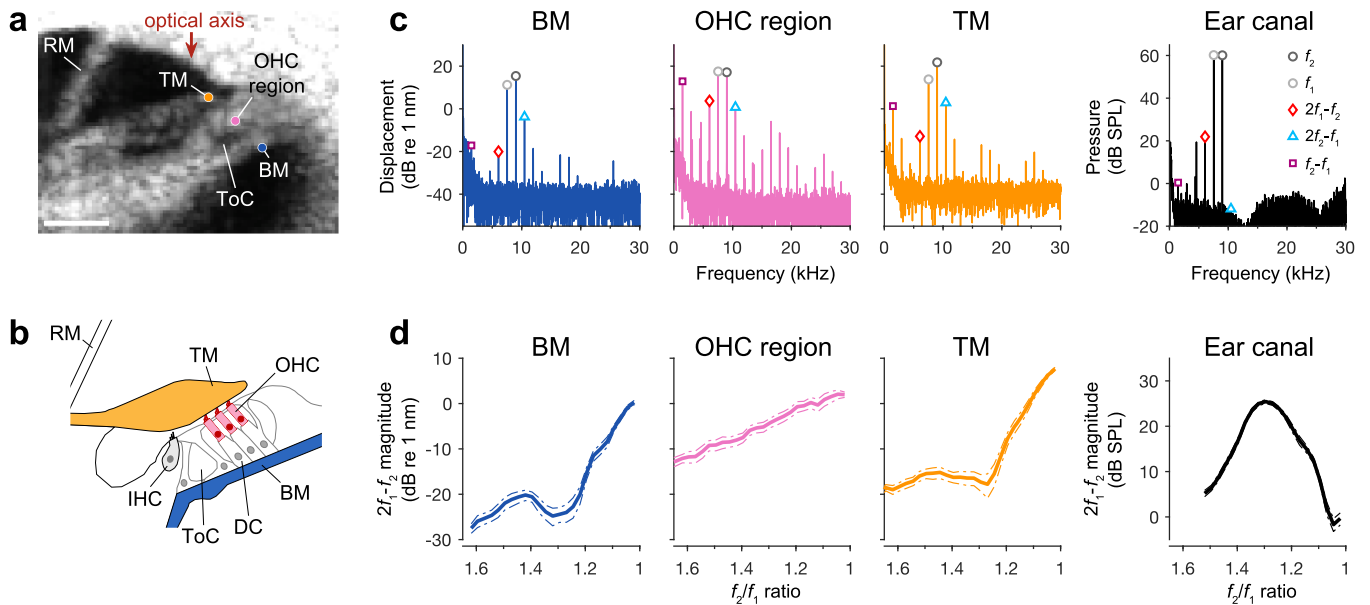

Fig. 9. Comparing intracochlear and ear canal DPs in mice. (a) OCT B-scan of an apical cochlear location in a wild-type CBA/CaJ mouse. RM = Reissner's membrane; ToC = tunnel of Corti. Scale bar = 100 μm. (b) Schematic of the OoC with relevant structures and regions labeled. IHC = inner hair cell; DC = Deiters' cell. (c) Spectra of BM, OHC region and TM displacements, as well as ear canal pressure, measured in response to two-tone stimuli in an individual mouse. Stimulus tones were presented at 60 dB SPL and with frequencies of 7.53 and 9 kHz (denoted f_1 and f_2, respectively). Responses at the stimulus frequencies and several DP frequencies are indicated by symbols. d. Average $2f_1$-f_2 DP magnitudes measured in BM, OHC region, and TM vibrations, as well as ear canal pressure, with $f_2 = 9$ kHz and f_1 varied to achieve different f_2/f_1 ratios. Data were obtained from eight mice, and averages are shown only when data from at least four mice were above the measurement noise floor. Dashed-dotted lines indicate ± 1 SE. Figure adapted from Dewey and Shera, 2023.

measured with a wide ratio (Fig. 10f). Although other interpretations are possible, the simplest explanation is that the SFOAE residual originates near the tonotopic location of the suppressor tone, potentially providing insight into cochlear mechanics at that site, particularly at low to mid probe intensities. While the characteristics of the wide ratio SFOAE residuals align with OoC vibrations at f_s = CF, how these vibrations stimulate the cochlear fluids to generate a backward OAE wave remains unclear (Charaziak, 2022).

2.10. Using vibration patterns in isolated gerbil cochleae to estimate relative stiffness values – Jong-Hoon Nam

Measurements of OoC deformation were used to estimate relative stiffnesses in the gerbil cochlea (Zhou et al., 2022). Measurements were made from excised gerbil cochleae after removing the bones between the objective lens and the OoC to enhance the optical resolution. Pressure-induced vibration measurements along two different optical axes allowed for reconstructing motion trajectories at four anatomical points (TM, RL, BM and DC), shown in Fig. 11a. From these trajectories, θ_{TM} (the direction of TM motion) and Δ_{TM}/Δ_{HB} (the ratio of
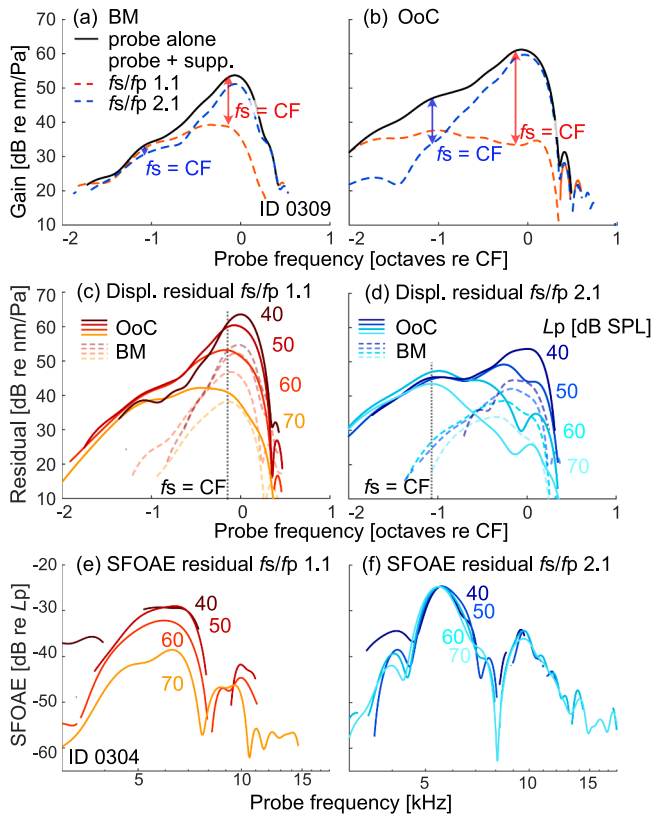
Fig. 10. Suppression of cochlear vibrations (a-d) and SFOAEs (e,f). Displacement gain functions measured in response to a 50-dB SPL probe frequency sweep presented alone (solid black) and in the presence of a 75-dB SPL suppressor at f_s/f_p ratios of 1.1 (dashed red) and 2.1 (dashed blue) are shown in panels (a) and (b) for BM and OoC motions, respectively. The corresponding displacement suppression residual functions are shown in panels (c) and (d) for f_s/f_p ratios of 1.1 and 2.1, respectively. BM data are plotted as dashed lines and OoC data as solid lines, across varying probe intensities from 40 to 70 dB SPL in 10 dB steps. Residual responses are calculated as a complex difference between the probe-alone responses and probe-with-suppressor conditions. Vertical dotted lines mark the condition where the suppressor frequency matches the CF of the preparation. The SFOAE gain functions (residual magnitude re stimulus level), measured for probe levels from 40 to 70 dB SPL, are shown in panels (e) and (f) for the 1.1 and 2.1 f_s/f_p ratio conditions in a different mouse. Experimental details are described in Charaziak and Pliso(2023).

displacements at the TM and hair bundle) were found. In Fig. 11b simulated results based on a finite element model (FEM) are shown together with measured results. The broken line and the shaded area show the measured mean and standard deviation of θ_{TM}. FEM simulations indicate that θ_{TM} and Δ_{TM}/Δ_{HB} are inversely proportional to the stiffness ratio between the TM and the hair bundle r_{TM} (= k_{TM}/k_{HB}). Using the measured values of Δ_{TM}/Δ_{HB} and θ_{TM}, the range of possible values for r_{TM} was found (Figs. 11c & d).

In Fig. 11e, axial deformations of the OHC and DC were measured after aligning the OCT optical axis with the cells' axis. In Fig. 11f, the broken line and the shaded area indicate the measured mean and standard deviation of θ_{DC}, the angle of motion at the joint between the OHC and DC. The solid blue and green lines are from simulations with different r_{DC} (= k_{DC}/k_{OHC}) values. Based on the FEM simulation, θ_{DC} depends on the axial stiffness ratio between OHC and DC. Using the measured values of (g) Δ_{DC}/Δ_{OHC} and (h) θ_{DC}, the range of possible values for r_{DC} was found (Figs. 11g & h).

These relative stiffness values are key to cochlear operation and to the development of cochlear models. The relative stiffness of the hair bundle and the TM allows predictions of the hair bundle pivoting that gives rise to MET. The relative stiffness of DC and pillar cells allows us to

predict the relationship between in vitro OHC electromotility and the in vivo effects of OHC electromotile forces.

3. Discussion

The integration of OCT imaging and vibrometry into hearing research has already produced significant advances in both animal research and human subjects (Kim et al., 2019; Lui et al., 2021; Monroy et al., 2015; Tan et al., 2018). The beauty of the OCT is its ability to measure both the vibrations from the surface of the cochlear partition, and reflective structures within. These intra-OoC observations show how active OHC motion interacts with surrounding structures, to investigate how the cochlear amplifier works. OCT allows for a more complete characterization of the relatively well-studied basal (high--frequency) region of the cochlea (Figs. 4, 5, & 7). Moreover, with its ability to measure through the bony capsule of the cochlea, OCT gives access to the relatively sparsely documented, apical (low-frequency) regions of the cochlea (Fig. 2) as well as the apical but still relatively high-frequency region in mice (Figs. 8& 9). The examples in this paper are a subset of observations made with OCT, and they illustrate some of the fundamental findings. Intra-OoC motions, particularly in the OHC region, differ from BM motion by exhibiting compressive nonlinearity throughout the sub-BF region (Figs. 2, 3, 7, and 10). At the RL, in the cochlear base, sub-BF nonlinearity has been observed in some preparations and approaches (Fig. 3, Ren et al., 2016) but not in all (Fig. 5, Cho and Puria, 2022). Because hair cell stereocilia are rooted in the RL, the motion of the RL is more closely tied to stereocilia stimulation than either BM or OHC motion, and quantifying RL motion and tuning is of central importance. This difference in findings could be due to different optical axes and different cochlear longitudinal locations, but could conceivably be related to misidentification, due to the localized OoC active region, and the fuzzy imaging of OCT. Future work will target such recently exposed uncertainties.

The finding of wideband nonlinearity is relevant to the study of OAEs. Pre-OCT, cochlear nonlinearity appeared to be restricted to the BF-peak, and OAEs were arguably a probe of activity in the BF-peak. With the OCT findings of wideband activity there is more reason to believe that cochlear regions basal to the peak contribute substantially to OAEs. This hypothesis was supported by the results of Fig. 10 (Charaziak, 2022). Fig. 9 compares intra-OoC DPs from the BM, TM and OHC (Dewey and Shera, 2023, 2024). The lack of clear correlation between these DPs and DPOAEs underscore the complexity of processes influencing the emergence of sound from the cochlea. The data on intra-OoC motion add pieces to the puzzle relating OAEs to intracochlear processes.

The findings of the two contributions exploring pathological conditions (loss of a row of OHCs in Fig. 8 (Xia et al., 2022), reduction of EP in Fig. 7 (Strimbu et al., 2020)) both indicate that the operation of the healthy cochlea relies on a synergy of processes. In Fig. 8, the loss of one row of OHCs (33 % of the total) resulted in a reduction of BM motion much larger than 33 %. In Fig. 7, OHC-region sub-BF activity recovered from low EP prior to the recovery of the BF peak, indicating that the presence of OHC activity was not by itself sufficient for the recovery of cochlear function – other more slowly recovering processes were also involved.

The apical measurements of OoC motion that are possible with OCT have shown that compared to the base, frequency responses in the OHC region and at the BM are more broadly tuned and the region of nonlinear BM responses is wider (Fig. 2, Meenderink and Dong, 2022; Meenderink et al., 2022). These observations indicate that the extent over which OHC forces affect OoC vibrations is broader in the apical cochlea. These data, together with low-frequency auditory nerve fiber (ANF) tuning curves (Joris et al., 2006; Versteegh et al., 2011), and low-frequency OAE recordings (Abdala et al., 2011; Shera et al., 2000) suggest that cochlear scaling invariance breaks down over almost 50 % of the cochlear length: apical biomechanics are not accurately described by
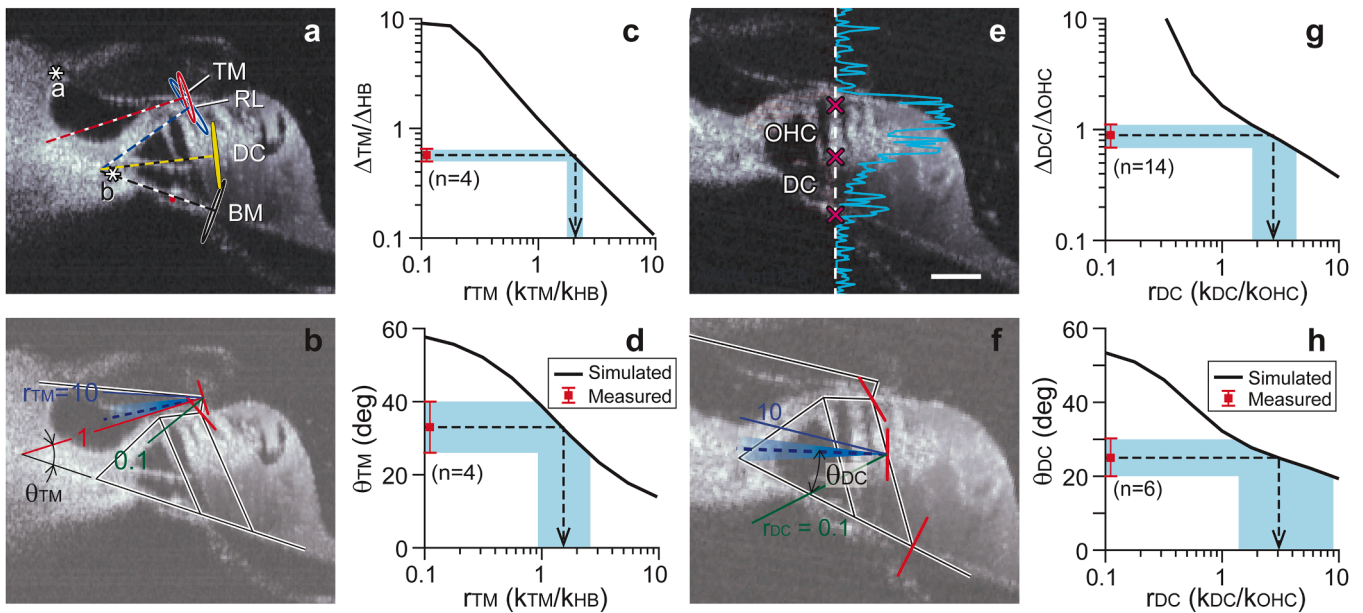
Fig. 11. (a) Motion trajectories at four anatomical points. (b) Simulated results shown together with measured data. The direction of TM motion (θ_{TM}) depends on the stiffness ratio between the TM and the hair bundle r_{TM} (=k_{TM}/k_{HB}). The broken line and the shaded area indicate the mean and standard deviation of θ_{TM}. (c, d) Parameter studies show that Δ_{TM}/Δ_{HB} (c) and θ_{TM} (d) are inversely proportional to r_{TM} and indicate the likely value of r_{TM}. Measured values are indicated as red square symbols and error bounds. The solid lines are from simulations with different r_{TM} values. (e) Axial deformations of the OHC and DC were measured after aligning the OCT optical axis with the cells' axis. (f) The angle of motion at the joint between OHC and DC, θ_{DC}, depends on the axial stiffness ratio between the OHC and DC, r_{DC} (=k_{DC}/k_{OHC}). Simulated results are shown together with measured data. The broken line and the shaded area indicate the mean and standard deviation of θ_{DC}. The solid lines are from simulations with different r_{DC} values. (g, h) Parameter studies of FE model simulations show that Δ_{DC}/Δ_{OHC} and θ_{DC} are inversely proportional to r_{DC}, and indicate the likely value of r_{DC}.

scaled versions of the high-frequency response (Shera et al., 2000).

Vibrometry in the low-frequency apical region of the cochlea, which is particularly relevant for human speech perception, recently generated some controversy with one study reporting a lack of tonotopicity and nearly constant group delays along the most apical ~25 % of the guinea pig cochlea (Burwood et al., 2022) while other studies have reported the presence of broad mechanical tuning and delays consistent with the presence of a traveling wave in guinea pigs, gerbils, and the chinchilla (Recio-Spinoso et al., 2023; Recio-Spinoso and Oghalai, 2017, 2018). The interpretation of these results is confounded by the issues discussed throughout this review: The relatively poorly delineated images in the apex makes structural identification difficult beyond coarse localization, and the complex motion of the OoC could include different tuning in the longitudinal, radial, and transverse directions. With this, calculating averaged OoC responses likely misrepresents the true nature of the response and could cause a misinterpretation of the tonotopic representation along the cochlear length (Burwood et al., 2022). Additional experiments by these groups and others will be needed before the matter is settled.

The study of Fig. 4 (Cooper et al., 2018) was one of the first to probe a region of the cochlea – the base of the gerbil – that had already been well-studied at the BM (Robles and Ruggero, 2001). Beyond observing and naming the "hotspot" of OHC-region motion, this study showed that the motion in the OHC region was substantially longitudinal and that the optical axis had a first-order influence on the phase of the findings. Fig. 2h, from the apex of the cochlea also emphasizes this, and in Fig. 6a correction for the skew caused by a longitudinal optical axis is described. One of the primary challenges and opportunities going forward is to devise experiments in which the 3-D nature of OoC motion is recognized. To this end, a 3D vibrometry system was recently developed to investigate the 3D motion of the OoC (Kim et al., 2022).

Finally, in Fig. 11 (Zhou et al., 2022) in vitro motions were measured in excised cochlear turns. With this reduced preparation a high numerical aperture objective lens could be used, sharpening up the fuzzy OCT images. Coupling the resulting high-resolution motion measurements with a physics-based finite element model of the in vitro preparation produced quantitative information about the mechanical properties of key cochlear structures – hair bundles, stereocilia, Deiters and pillar cells. This information is needed to develop more accurate cochlear traveling wave models. With these more accurate models, the wealth of new in vivo data coming out of OCT-based measurements can be used to advance our understanding of cochlear operation and cochlear amplification.

4. Conclusion

Through these examples, 3-D OoC motion and image resolution have been noted as ongoing challenges to the interpretation of OCT-based measurements. In addition to these challenges, the fundamental working of OCT and heterodyne interferometry can lead to artifactual findings. OCT and heterodyne interferometry are sensitive to path length, which changes due to the motion of the structure under investigation – this is the way we use interferometry to measure motion. But path length can also change for other reasons, for example due to changes in index of refraction (which could occur if sound stimulation caused changes in mechanical properties) and due to changes in fluid depth. This latter is of concern for measurements made through the RW, and by measuring RW membrane motion, corrections can be made if necessary. In addition, for both heterodyne interferometry and OCT, we interpret motion measured at a point – the point being the laser focal point in heterodyne interferometry, and a pixel in the A-scan for OCT – and assume that the measurement is uninfluenced by motions at nearby locations. This assumption can be confounded if nearby locations are much more reflective than the chosen point, in which case "phase leakage" leads to errors in the reported motion (de La Rochefoucauld et al., 2005; Lin et al., 2017). For this, interpretative care must be taken when motion is measured from relatively dim points. Some of the challenges of OCT will be addressed with technological advances. Wider bandwidth light

sources will improve spatial resolution and reduce the possibility for phase leakage. Contrast enhancement techniques such as dynamic OCT are under active development and have been applied to the cochlea (Ren et al., 2024; Serafino et al., 2024).

OCT provides detailed insights into the motions within the OC, allowing further exploration of cochlear micro-mechanics in both normal and impaired ears. These observations allow the development of more accurate models to fully comprehend cochlear mechanics, and lead to improvements in clinical diagnostic tools and treatment strategies.

For access to the data displayed in the figures in this paper please contact the author(s) of that figure.

CRediT authorship contribution statement

Elizabeth S. Olson: Writing – original draft, Project administration, Methodology, Investigation, Funding acquisition, Formal analysis, Conceptualization. **Wei Dong:** Writing – review & editing, Supervision, Project administration, Methodology, Investigation, Funding acquisition, Formal analysis, Conceptualization. **Brian E. Applegate:** Writing – review & editing, Supervision, Software, Project administration, Methodology, Investigation, Funding acquisition, Formal analysis, Conceptualization. **Karolina K. Charaziak:** Writing – review & editing, Supervision, Project administration, Methodology, Investigation, Funding acquisition, Formal analysis, Conceptualization. **James B. Dewey:** Writing – review & editing, Project administration, Methodology, Investigation, Funding acquisition, Formal analysis, Conceptualization. **Brian L. Frost:** Writing – review & editing, Software, Methodology, Investigation, Funding acquisition, Formal analysis, Conceptualization. **Sebastiaan W.F. Meenderink:** Software, Methodology, Investigation, Formal analysis, Conceptualization. **Jong-Hoon Nam:** Writing – review & editing, Supervision, Project administration, Methodology, Investigation, Funding acquisition, Formal analysis, Conceptualization. **John S. Oghalai:** Writing – review & editing, Supervision, Project administration, Methodology, Investigation, Funding acquisition, Formal analysis, Conceptualization. **Sunil Puria:** Writing – review & editing, Supervision, Project administration, Methodology, Investigation, Funding acquisition, Formal analysis, Conceptualization. **Tianying Ren:** Writing – review & editing, Supervision, Project administration, Methodology, Investigation, Funding acquisition, Formal analysis, Conceptualization. **C. Elliott Strimbu:** Writing – review & editing, Methodology, Investigation, Formal analysis, Conceptualization. **Marcel van der Heijden:** Writing – review & editing, Supervision, Software, Project administration, Methodology, Investigation, Funding acquisition, Formal analysis, Conceptualization.

IV. Appendix - Additional Reading

The ten examples shown above represent just a subset of the work produced. For a previous review, see (Olson and Strimbu, 2020). Additional recommended readings on OCT vibrometry in the cochlea are listed below.

1. Basal cochlea (all species)

Fallah, E., Strimbu, C. E., & Olson, E. S. (2019). Nonlinearity and amplification in cochlear responses to single and multi-tone stimuli.

Fallah, E., Strimbu, C. E., & Olson, E. S. (2021). Nonlinearity of intracochlear motion and local cochlear microphonic: Comparison between guinea pig and gerbil.

He, W., & Ren, T. (2021). The origin of mechanical harmonic distortion within the organ of Corti in living gerbil cochleae.

He, W., Burwood, G., Fridberger, A., Nuttall, A. L., & Ren, T. (2022). An outer hair cell-powered global hydromechanical mechanism for cochlear amplification.

He, W., Burwood, G., Porsov, E. V., Fridberger, A., Nuttall, A. L., & Ren, T. (2022). The reticular lamina and basilar membrane vibrations in the transverse direction in the basal turn of the living gerbil cochlea.

Ren, T., He, W., & Barr-Gillespie, P. G. (2016). Reverse transduction measured in the living cochlea by low-coherence heterodyne interferometry.

Strimbu CE and Olson ES (2022). Salicylate-induced changes in organ of Corti vibrations.

Strimbu CE, Chiriboga LA, Frost BL, Olson ES. (2024) Regional differences in cochlear nonlinearity across the basal organ of Corti of gerbil. van der Heijden, M., & Vavakou, A. (2022). Rectifying and sluggish: Outer hair cells as regulators rather than amplifiers.

Vavakou, A., Cooper, N. P., & van der Heijden, M. (2019). The frequency limit of outer hair cell motility measured in vivo.

2. Apical cochlea (not mice)

Burwood, G., Hakizimana, P., Nuttall, A. L., & Fridberger, A. (2022). Best frequencies and temporal delays are similar across the low-frequency regions of the guinea pig cochlea.

Burwood, G., He, W. X., Fridberger, A., Ren, T. Y., & Nuttall, A. L. (2022). Outer hair cell driven reticular lamina mechanical distortion in living cochleae.

Dong, W., Xia, A., Puria, S., Applegate, B. E., & Oghalai, J. S. (2017). Organ of Corti Tuning within the 2nd Apical Turn of the Intact Gerbil Cochlea

Dong, W., Xia, A., Raphael, P. D., Puria, S., Applegate, B. E., & Oghalai, J. S. (2018). Organ of Corti vibration within the intact gerbil cochlea measured by volumetric optical coherence tomography and vibrometry.

Recio-Spinoso, A., Dong, W., & Oghalai, J. S. (2023). On the Tonotopy of the Low-Frequency Region of the Cochlea.

Recio-Spinoso, A., & Oghalai, J. S. (2018). Unusual mechanical processing of sounds at the apex of the Guinea pig cochlea.

Recio-Spinoso, A., & Oghalai, J. S. (2017). Mechanical tuning and amplification within the apex of the guinea pig cochlea.

3. Apical cochlea (mice)

Dewey, J. B. (2022). Cubic and quadratic distortion products in vibrations of the mouse cochlear apex.

Dewey, J. B., Altoe, A., Shera, C. A., Applegate, B. E., & Oghalai, J. S. (2021). Cochlear outer hair cell electromotility enhances organ of Corti motion on a cycle-by-cycle basis at high frequencies in vivo.

Dewey, J. B., Applegate, B. E., & Oghalai, J. S. (2019). Amplification and Suppression of Traveling Waves along the Mouse Organ of Corti: Evidence for Spatial Variation in the Longitudinal Coupling of Outer Hair Cell-Generated Forces.

Dewey, J. B., & Shera, C. A. (2023). Bandpass Shape of Distortion-Product Otoacoustic Emission Ratio Functions Reflects Cochlear Frequency Tuning in Normal-Hearing Mice.

Lee, H. Y., Raphael, P. D., Xia, A., Kim, J., Grillet, N., Applegate, B. E., … Oghalai, J. S. (2016). Two-Dimensional Cochlear Micromechanics Measured In Vivo Demonstrate Radial Tuning within the Mouse Organ of Corti.

4. In vitro

Lin, WC., Macić, A., Becker, J. and Nam, J-H. (2024). Asymmetric vibrations in the organ of Corti by outer hair cells measured from excised gerbil cochlea.

Jabeen, T., Holt, J.C., Becker, J.R. and Nam, J-H. (2020). Interactions between Passive and Active Vibrations in the Organ of Corti In Vitro.

5. Models

Altoe, A., Dewey, J. B., Charaziak, K. K., Oghalai, J. S., & Shera, C. A. (2022). Overturning the mechanisms of cochlear amplification via area deformations of the organ of Corti.

Guinan, J. J., Jr. (2022). Cochlear amplification in the short-wave region by outer hair cells changing organ-of-Corti area to amplify the fluid traveling wave.

Samaras, G., Wen, H., & Meaud, J. (2023). Broad nonlinearity in reticular lamina vibrations requires compliant organ of Corti structures.

Data availability

Data will be made available on request.

References

Abdala, C., Dhar, S., Kalluri, R., 2011. Deviations from scaling symmetry in the apical half of the human cochlea. AIP. Conf. Proc. 1403, 483–488. https://doi.org/10.1063/1.3658135.

Altoe, A., Dewey, J.B., Charaziak, K.K., Oghalai, J.S., Shera, C.A., 2022. Overturning the mechanisms of cochlear amplification via area deformations of the organ of Corti. J. Acoust. Soc. Am. 152 (4), 2227. https://doi.org/10.1121/10.0014794.

Applegate, B.E., Shelton, R.L., Gao, S.S., Oghalai, J.S., 2011. Imaging high-frequency periodic motion in the mouse ear with coherently interleaved optical coherence tomography. Opt. Lett. 36 (23), 4716–4718. https://doi.org/10.1364/OL.36.004716.

Aumann, S., Donner, S., Fischer, J., Muller, F., 2019. Optical Coherence Tomography (OCT): Principle and Technical Realization, in: Bille, J.F. (Ed.) High Resolution Imaging in Microscopy and Ophthalmology: New Frontiers in Biomedical Optics. Cham (CH), pp. 59–85.

Burwood, G., Hakizimana, P., Nuttall, A.L., Fridberger, A., 2022. Best frequencies and temporal delays are similar across the low-frequency regions of the guinea pig cochlea. Sci. Adv. 8 (38), eabq2773. https://doi.org/10.1126/sciadv.abq2773.

Charaziak, K.K., 2022. Suppression of organ-of-Corti vibrations and otoacoustic emissions in mice, in: Dong, W., Epp, B. (Eds.), Mechanics of Hearing Workshop, c2024 ed. AIP Conf. Proc., Helsingør, Denmark, p. 060006.

Charaziak, K.K., Pliso, M., 2023. Tracing the origins of otoacoustic emissions to inner-ear vibrations in vivo, the 29th International Congress on Sound and Vibration. Prague; Czech Republic.

Cho, N.H., Puria, S., 2022. Cochlear motion across the reticular lamina implies that it is not a stiff plate. Sci. Rep. 12 (1), 18715. https://doi.org/10.1038/s41598-022-23525-x.

Choudhury, N., Song, G., Chen, F., Matthews, S., Tschinkel, T., Zheng, J., Jacques, S.L., Nuttall, A.L., 2006. Low coherence interferometry of the cochlear partition. Hear. Res. 220 (1–2), 1–9. https://doi.org/10.1016/j.heares.2006.06.006.

Cooper, N.P., Vavakou, A., van der Heijden, M., 2018. Vibration hotspots reveal longitudinal funneling of sound-evoked motion in the mammalian cochlea. Nat. Commun. 9 (1), 3054. https://doi.org/10.1038/s41467-018-05483-z.

de La Rochefoucauld, O., Khanna, S.M., Olson, E.S., 2005. Recording depth and signal competition in heterodyne interferometry. J. Acoust. Soc. Am. 117 (3 Pt 1), 1267–1284. https://doi.org/10.1121/1.1848177.

Dewey, J.B., Altoe, A., Shera, C.A., Applegate, B.E., Oghalai, J.S., 2021. Cochlear outer hair cell electromotility enhances organ of Corti motion on a cycle-by-cycle basis at high frequencies in vivo. Proc. Natl. Acad. Sci. U.S.A. 118 (43). https://doi.org/10.1073/pnas.2025206118.

Dewey, J.B., Applegate, B.E., Oghalai, J.S., 2019. Amplification and suppression of traveling waves along the mouse organ of Corti: evidence for spatial variation in the longitudinal coupling of outer hair cell-generated forces. J. Neurosci. 39 (10), 1805–1816. https://doi.org/10.1523/JNEUROSCI.2608-18.2019.

Dewey, J.B., Shera, C.A., 2023. Bandpass shape of distortion-product otoacoustic emission ratio functions reflects cochlear frequency tuning in normal-hearing mice. J. Assoc. Res. Otolaryngol. JARO 24 (3), 305–324. https://doi.org/10.1007/s10162-023-00892-4.

Dewey, J.B., Shera, C.A., 2024. Similar tuning of distortion-product otoacoustic emission ratio functions and cochlear vibrations in mice. AIP. Conf. Proc. 3062 (1). https://doi.org/10.1063/5.0195534.

Frost, B.L., Strimbu, C.E., Olson, E.S., 2022. Using volumetric optical coherence tomography to achieve spatially resolved organ of Corti vibration measurements. J. Acoust. Soc. Am. 151 (2), 1115. https://doi.org/10.1121/10.0009576.

Frost, B.L., Strimbu, C.E., Olson, E.S., 2023. Reconstruction of transverse-longitudinal vibrations in the organ of Corti complex via optical coherence tomography. J. Acoust. Soc. Am. 153 (2), 1347. https://doi.org/10.1121/10.0017345.

Gao, S.S., Wang, R., Raphael, P.D., Moayedi, Y., Groves, A.K., Zuo, J., Applegate, B.E., Oghalai, J.S., 2014. Vibration of the organ of Corti within the cochlear apex in mice. J. Neurophysiol. 112 (5), 1192–1204. https://doi.org/10.1152/jn.00306.2014.

Guinan Jr., J.J., 2022. Cochlear amplification in the short-wave region by outer hair cells changing organ-of-Corti area to amplify the fluid traveling wave. Hear. Res. 426, 108641. https://doi.org/10.1016/j.heares.2022.108641.

He, W., Kemp, D., Ren, T., 2018. Timing of the reticular lamina and basilar membrane vibration in living gerbil cochleae. Elife 7. https://doi.org/10.7554/eLife.37625.

Hong, S.S., Freeman, D.M., 2006. Doppler optical coherence microscopy for studies of cochlear mechanics. J. Biomed. Opt. 11 (5), 054014. https://doi.org/10.1117/1.2358702.

Huang, D., Swanson, E.A., Lin, C.P., Schuman, J.S., Stinson, W.G., Chang, W., Hee, M.R., Flotte, T., Gregory, K., Puliafito, C.A., et al., 1991. Optical coherence tomography. Science (1979) 254 (5035), 1178–1181. https://doi.org/10.1126/science.1957169.

Joris, P.X., van de Sande, B., Recio-Spinoso, A., van der Heijden, M., 2006. Auditory midbrain and nerve responses to sinusoidal variations in interaural correlation. J. Neurosci. 26 (1), 279–289.

Khanna, S.M., Hao, L.F., 1999. Reticular lamina vibrations in the apical turn of a living guinea pig cochlea. Hear. Res. 132 (1–2), 15–33. https://doi.org/10.1016/s0378-5955(99)00027-1.

Kim, W., Kim, S., Huang, S., Oghalai, J.S., Applegate, B.E., 2019. Picometer scale vibrometry in the human middle ear using a surgical microscope based optical coherence tomography and vibrometry system. Biomed. Opt. Express. 10 (9), 4395–4410. https://doi.org/10.1364/BOE.10.004395.

Kim, W., Liu, D., Kim, S., Ratnayake, K., Macias-Escriva, F., Mattison, S., Oghalai, J.S., Applegate, B.E., 2022. Vector of motion measurements in the living cochlea using a 3D OCT vibrometry system. Biomed. Opt. Express. 13 (4), 2542–2553. https://doi.org/10.1364/BOE.451537.

Lee, H.Y., Raphael, P.D., Xia, A., Kim, J., Grillet, N., Applegate, B.E., Ellerbee Bowden, A. K., Oghalai, J.S., 2016. Two-dimensional cochlear micromechanics measured in vivo demonstrate radial tuning within the mouse organ of Corti. J. Neurosci. 36 (31), 8160–8173. https://doi.org/10.1523/JNEUROSCI.1157-16.2016.

Lin, N.C., Fallah, E., Strimbu, C.E., Hendon, C.P., Olson, E.S., 2019. Scanning optical coherence tomography probe for in vivo imaging and displacement measurements in the cochlea. Biomed. Opt. Express. 10 (2), 1032–1043. https://doi.org/10.1364/BOE.10.001032.

Lin, N.C., Hendon, C.P., Olson, E.S., 2017. Signal competition in optical coherence tomography and its relevance for cochlear vibrometry. J. Acoust. Soc. Am. 141 (1), 395. https://doi.org/10.1121/1.4973867.

Lui, C.G., Kim, W., Dewey, J.B., Macias-Escriva, F.D., Ratnayake, K., Oghalai, J.S., Applegate, B.E., 2021. In vivo functional imaging of the human middle ear with a hand-held optical coherence tomography device. Biomed. Opt. Express. 12 (8), 5196–5213. https://doi.org/10.1364/BOE.430935.

Meenderink, S.W.F., Dong, W., 2022. Organ of Corti vibrations are dominated by longitudinal motion in vivo. Commun. Biol. 5 (1), 1285. https://doi.org/10.1038/s42003-022-04234-7.

Meenderink, S.W.F., Lin, X., Park, B.H., Dong, W., 2022. Sound Induced Vibrations Deform the Organ of Corti Complex in the Low-Frequency Apical Region of the Gerbil Cochlea for Normal Hearing: sound Induced Vibrations Deform the Organ of Corti Complex. J. Assoc. Res. Otolaryngol. 23 (5), 579–591. https://doi.org/10.1007/s10162-022-00856-0.

Monroy, G.L., Shelton, R.L., Nolan, R.M., Nguyen, C.T., Novak, M.A., Hill, M.C., McCormick, D.T., Boppart, S.A., 2015. Noninvasive depth-resolved optical measurements of the tympanic membrane and middle ear for differentiating otitis media. Laryngoscope 125 (8), E276–E282. https://doi.org/10.1002/lary.25141.

Olson, E.S., Strimbu, C.E., 2020. Cochlear mechanics: new insights from vibrometry and Optical Coherence Tomography. Curr. Opin. Physiol. 18, 56–62. https://doi.org/10.1016/j.cophys.2020.08.022.

Recio-Spinoso, A., Dong, W., Oghalai, J.S., 2023. On the Tonotopy of the Low-Frequency Region of the Cochlea. J. Neurosci. 43 (28), 5172–5179. https://doi.org/10.1523/JNEUROSCI.0249-23.2023.

Recio-Spinoso, A., Oghalai, J.S., 2017. Mechanical tuning and amplification within the apex of the guinea pig cochlea. J. Physiol. 595 (13), 4549–4561. https://doi.org/10.1113/JP273881.

Recio-Spinoso, A., Oghalai, J.S., 2018. Unusual mechanical processing of sounds at the apex of the Guinea pig cochlea. Hear. Res. 370, 84–93. https://doi.org/10.1016/j.heares.2018.09.009.

Ren, C., Hao, S., Wang, F., Matt, A., Amaral, M.M., Yang, D., Wang, L., Zhou, C., 2024. Dynamic contrast optical coherence tomography (DyC-OCT) for label-free live cell imaging. Commun. Biol. 7 (1), 278. https://doi.org/10.1038/s42003-024-05973-5.

Ren, T., He, W., Kemp, D., 2016. Reticular lamina and basilar membrane vibrations in living mouse cochleae. Proc. Natl. Acad. Sci. u S a 113 (35), 9910–9915. https://doi.org/10.1073/pnas.1607428113.

Robles, L., Ruggero, M.A., 2001. Mechanics of the mammalian cochlea. Physiol. Rev. 81 (3), 1305–1352. https://doi.org/10.1152/physrev.2001.81.3.1305.

Ruggero, M.A., Robles, L., Rich, N.C., 1992. Two-tone suppression in the basilar membrane of the cochlea: mechanical basis of auditory-nerve rate suppression. J. Neurophysiol. 68 (4), 1087–1099. https://doi.org/10.1152/jn.1992.68.4.1087.

Samaras, G., Wen, H., Meaud, J., 2023. Broad nonlinearity in reticular lamina vibrations requires compliant organ of Corti structures. Biophys. J. 122 (5), 880–891. https://doi.org/10.1016/j.bpj.2023.01.029.

Schmiedt, R.A., 1989. Spontaneous rates, thresholds and tuning of auditory-nerve fibers in the gerbil: comparisons to cat data. Hear. Res. 42 (1), 23–35. https://doi.org/10.1016/0378-5955(89)90115-9.

Serafino, M.J., Walker, C., Quiñones, P.M., Wang, J., Macías-Escrivá, F.D., Oghalai, J.S., Applegate, B.E., 2024. Dynamic optical coherence tomography strongly enhances contrast in the ex vivo murine cochlea. Opt. Coherence Tomogr. Coherence Domain Optical Methods in Biomed. XXVIII. SPIE, 155–157.

Shera, C.A., Talmadge, C.L., Tubis, A., 2000. Interrelations among distortion-product phase-gradient delays: their connection to scaling symmetry and its breaking. J. Acoust. Soc. Am. 108 (6), 2933–2948.

Siegel, J.H., Cerka, A.J., Recio-Spinoso, A., Temchin, A.N., van Dijk, P., Ruggero, M.A., 2005. Delays of stimulus-frequency otoacoustic emissions and cochlear vibrations contradict the theory of coherent reflection filtering. J. Acoust. Soc. Am. 118 (4), 2434–2443. https://doi.org/10.1121/1.2005867.

Sirjani, D.B., Salt, A.N., Gill, R.M., Hale, S.A., 2004. The influence of transducer operating point on distortion generation in the cochlea. J. Acoust. Soc. Am. 115 (3), 1219–1229. https://doi.org/10.1121/1.1647479.

Strimbu, C.E., Wang, Y., Olson, E.S., 2020. Manipulation of the endocochlear potential reveals two distinct types of cochlear nonlinearity. Biophys. J. 119 (10), 2087–2101. https://doi.org/10.1016/j.bpj.2020.10.005.

Tan, H.E.I., Santa Maria, P.L., Wijesinghe, P., Francis Kennedy, B., Allardyce, B.J., Eikelboom, R.H., Atlas, M.D., Dilley, R.J., 2018. Optical coherence tomography of the tympanic membrane and middle ear: a review. Otolaryngol. Head. Neck. Surg. 159 (3), 424–438. https://doi.org/10.1177/0194599818775711.

Tearney, G.J., Brezinski, M.E., Bouma, B.E., Boppart, S.A., Pitris, C., Southern, J.F., Fujimoto, J.G., 1997. In vivo endoscopic optical biopsy with optical coherence tomography. Science (1979) 276 (5321), 2037–2039. https://doi.org/10.1126/science.276.5321.2037.

Versteegh, C.P., Meenderink, S.W., van der Heijden, M., 2011. Response characteristics in the apex of the gerbil cochlea studied through auditory nerve recordings. J. Assoc. Res. Otolaryngol. JARO 12 (3), 301–316. https://doi.org/10.1007/s10162-010-0255-y.

Wang, Y., Fallah, E., Olson, E.S., 2019. Adaptation of cochlear amplification to low endocochlear potential. Biophys. J. 116 (9), 1769–1786. https://doi.org/10.1016/j.bpj.2019.03.020.

Xia, A., Udagawa, T., Quinones, P.M., Atkinson, P.J., Applegate, B.E., Cheng, A.G., Oghalai, J.S., 2022. The impact of targeted ablation of one row of outer hair cells and Deiters' cells on cochlear amplification. J. Neurophysiol. 128 (5), 1365–1373. https://doi.org/10.1152/jn.00501.2021.

Zhou, W., Jabeen, T., Sabha, S., Becker, J., Nam, J.H., 2022. Deiters cells act as mechanical equalizers for outer hair cells. J. Neurosci. 42 (44), 8361–8372. https://doi.org/10.1523/JNEUROSCI.2417-21.2022.